**Proceedings of the 7th GACM Colloquium on Computational Mechanics
for Young Scientists from Academia and Industry
October 11-13, 2017 in Stuttgart, Germany**

Parallel Stabilized FEM for the Flow Simulations of Microstructured Fluids

Metin Cakircali[1,2,*] and Marek Behr[2]

Micro Abstract
The Single-Walled Carbon Nanotubes (SWNT) have unique properties that make them ideal for nano-materials. We use efficient numerical methods to improve our understanding of the macroscale assembly processes (e.g., fiber spinning). The Galerkin/Least-Squares formulation is derived for the fully coupled transient equation systems. Space-time elements with equal order velocity-pressure-order parameter are used for several relevant test cases. The results are compared with available literature data.

[1]Institute for Advanced Simulation (IAS) / Jülich Supercomputing Centre (JSC), JARA-HPC, Forschungszentrum Jülich GmbH, Jülich, Germany

[2]Chair for Computational Analysis of Technical Systems, JARA-HPC, RWTH Aachen University, Aachen, Germany

***Corresponding author**: m.cakircali@fz-juelich.de

Introduction

Single-Walled Carbon Nanotubes (SWNTs) demonstrate unique properties at molecular scales [9], which makes them ideal candidates for manufacturing multifunctional materials at macro-scales [1–3]. The main difficulty in assembly processes is to produce macro-scale materials that exhibit the same unique properties as the SWNTs. The fiber spinning process is a viable production method that uses the SWNT solutions as liquid. In order to sustain the unique properties at macro-scales, the fibers must be formed by long, highly aligned, and defect-free arrangements of nanotubes [2]. SWNTs are considered as rigid rod-like polymers, and at high concentrations, they form liquid crystals (nematic phase) that allow the fiber formation [6, 8]. The viscoelastic fluids are commonly modeled by constitutive equations that relate the stress tensor and kinematic tensors (e.g., rate-of-strain tensor). The constitutive equations for microstructured liquids are derived from molecular and kinetic theories in order to retain the micro-macro features of the flow. The dynamic behavior of rod-like molecules have been extensively studied over the last decades [5, 7, 13]. Here [11] we use the constitutive model that was developed for the liquid-crystalline polymers (LCPs). The model adds the long-range elasticity (proposed by [12]) to the Doi theory [7]. The microstructured liquid model consists of mass, momentum and constitutive equations in differential form. The momentum and constitutive equations are fully coupled via the extra-stress equation. We solve the system of equations using a parallel stabilized finite element method [4, 14]. The "order parameter-velocity-pressure" Galerkin/Least-Squares formulation (GLS3) is derived for the space-time elements as well as for the semi-discrete form. The nonlinear equations are solved iteratively by Newton-Raphson (NR) scheme. The parallel implementation is purely via message-passing communication library, MPI.

1 Governing Equations

The governing equations for the microstructured liquids consist of momentum, continuity, and constitutive equations. Additionally, an extra-stress equation is needed for fully coupling the momentum and the constitutive equations. In the current study, we use the non-dimensional form of the equations. The length and velocity are scaled by the characteristic length H and the

characteristic velocity V, respectively.

1.1 Flow equations

The transient incompressible Navier-Stokes fluid can be written as,

$$\mathrm{Re}\left(\frac{\partial \boldsymbol{u}}{\partial t} + \boldsymbol{u}\cdot\boldsymbol{\nabla}\boldsymbol{u}\right) - \boldsymbol{\nabla}\cdot\boldsymbol{\sigma} = \boldsymbol{0}, \tag{1}$$

$$\boldsymbol{\nabla}\cdot\boldsymbol{u} = \boldsymbol{0}, \tag{2}$$

where Re is the Reynolds number, $\boldsymbol{u}$ is the velocity, and $\boldsymbol{\sigma}$ is the total stress tensor that is defined as,

$$\boldsymbol{\sigma} = -p\boldsymbol{\delta} + \boldsymbol{\tau}, \tag{3}$$

where p is the pressure, $\boldsymbol{\delta}$ is the unit tensor, and $\boldsymbol{\tau}$ is the extra-stress tensor. The Reynolds number Re is the ratio between the inertial forces and the other forces that is defined as,

$$\mathrm{Re} = \frac{\rho V^2}{c k_{\mathrm{B}} T}, \tag{4}$$

where c is the number of entanglements per unit volume, and $k_B T$ is the Boltzmann's constant times the absolute temperature.

1.2 Constitutive equation

The constitutive equation for the microstructured liquids in nematic phase is written as,

$$\frac{\partial \boldsymbol{S}}{\partial t} + \boldsymbol{u}\cdot\boldsymbol{\nabla}\boldsymbol{S} = \boldsymbol{F}^{\mathrm{h}}(\boldsymbol{S}) + \boldsymbol{F}^{\mathrm{nh}}(\boldsymbol{S}) + \boldsymbol{G}(\boldsymbol{S}), \tag{5}$$

$$\boldsymbol{F}^{\mathrm{h}}(\boldsymbol{S}) = \frac{1}{\mathrm{De}}\left[(3U-4)\boldsymbol{S} + 6U\boldsymbol{S}\cdot\boldsymbol{S} - 6U(\boldsymbol{S}:\boldsymbol{S})\left(\boldsymbol{S} + \frac{1}{2}\boldsymbol{\delta}\right)\right], \tag{6}$$

$$\boldsymbol{F}^{\mathrm{nh}}(\boldsymbol{S}) = \frac{1}{\mathrm{Er}}\left\{(\boldsymbol{\nabla}^2\boldsymbol{S}) + (\boldsymbol{\nabla}^2\boldsymbol{S})\cdot\boldsymbol{S} + \boldsymbol{S}\cdot(\boldsymbol{\nabla}^2\boldsymbol{S}) - 2\left[(\boldsymbol{\nabla}^2\boldsymbol{S}):\boldsymbol{S}\right]\left(\boldsymbol{S} + \frac{1}{2}\boldsymbol{\delta}\right)\right\}, \tag{7}$$

$$\boldsymbol{G}(\boldsymbol{S}) = \frac{1}{2}\left(\boldsymbol{\kappa} + \boldsymbol{\kappa}^T\right) + \boldsymbol{S}\cdot\boldsymbol{\kappa}^T + \boldsymbol{\kappa}\cdot\boldsymbol{S} - 2\left(\boldsymbol{\kappa}:\boldsymbol{S}\right)\left(\boldsymbol{S} + \frac{1}{2}\boldsymbol{\delta}\right), \tag{8}$$

$$\boldsymbol{\kappa} = \boldsymbol{\omega}(\boldsymbol{u}) + \lambda\boldsymbol{\varepsilon}(\boldsymbol{u}), \tag{9}$$

where $\boldsymbol{S}$ is the (symmetric and traceless) order parameter tensor, $\boldsymbol{\omega}$ is the vorticity tensor, $\boldsymbol{\varepsilon}$ is the rate-of-strain tensor, and U is the nematic potential. The parameter λ,

$$\lambda = (r^2-1)/(r^2+1), \tag{10}$$

is related to the tumbling period of the rod-like molecules, where r is the molecular aspect ratio. The Deborah number,

$$\mathrm{De} = \frac{V/H}{\bar{D}_{\mathrm{R}}}, \tag{11}$$

is the ratio of the molecular (relaxation) time scale $1/\bar{D}_R$ to the characteristic time scale of the flow, where $\bar{D}_{\mathrm{R}}$ is a constant that averages the characteristic rotational diffusion coefficient D_{R}. The Ericksen number is the ratio of the viscous stress (short range nematic potential) and elastic stress (long range Marrucci-Greco potential), which is written as,

$$\mathrm{Er} = \frac{8}{U}\left(\frac{H}{R}\right)^2 \mathrm{De}, \tag{12}$$

where R is the characteristic molecular interaction distance.
The inter-molecular kinetics, separated into homogeneous and non-homogeneous parts, are collected in Eqs. (6) and (7), respectively. The molecular advection terms are collected in Eq. (8).

1.3 Extra-stress equation (coupling)

The momentum equation (1) is coupled to the constitutive equation (5) via the extra-stress equation,

$$\boldsymbol{\tau} = -\frac{1}{2}\lambda \mathrm{De}\boldsymbol{F}(\boldsymbol{S}) + \frac{1}{2}\frac{\mathrm{De}}{\mathrm{Er}}\left[(\boldsymbol{\nabla}^2\boldsymbol{S})\cdot\boldsymbol{S} - \boldsymbol{S}\cdot(\boldsymbol{\nabla}^2\boldsymbol{S})\right] + 2\nu_s\boldsymbol{\varepsilon}(\boldsymbol{u}), \tag{13}$$

where the dimensionless parameter ν_s,

$$\nu_s = \frac{\mu_s(V/H)}{ck_BT}, \tag{14}$$

is the ratio of the solvent viscosity μ_s and the characteristic polymer viscosity. The second term in Eq. (13) is the antisymmetric part of the stress tensor. The asymmetry implies that the gradients in the orientation generate torques on the molecules.

2 GLS3 formulation

The weak form of the governing equations, (1), (2) and (5), for the linear space-time elements with three unknowns $\boldsymbol{S}$, $\boldsymbol{u}$, and p can be written as,

$$\begin{aligned}
&\int_Q \boldsymbol{w}\cdot\mathrm{Re}\left(\frac{\partial\boldsymbol{u}}{\partial t} + \boldsymbol{u}\cdot\boldsymbol{\nabla}\boldsymbol{u}\right)dQ - \int_Q \boldsymbol{\nabla}\cdot\boldsymbol{w}\,p\,dQ - \int_Q \boldsymbol{w}\cdot\boldsymbol{\nabla}\cdot\boldsymbol{\tau}\,dQ \\
&\quad + \int_Q q\,\boldsymbol{\nabla}\cdot\boldsymbol{u}\,dQ - \int_P \boldsymbol{w}\cdot\boldsymbol{h}\,dP + \int_\Omega \boldsymbol{w}^+\cdot\mathrm{Re}\left(\boldsymbol{u}^+ - \boldsymbol{u}^-\right)d\Omega \\
&\quad + \sum_{e=1}^{n_{el}}\int_{Q^e}\frac{\tau_{\mathrm{MOM}}}{\mathrm{Re}}\left[\mathrm{Re}\left(\frac{\partial\boldsymbol{w}}{\partial t} + \boldsymbol{u}\cdot\boldsymbol{\nabla}\boldsymbol{w}\right) + \boldsymbol{\nabla}q\right] \\
&\quad \cdot\left[\mathrm{Re}\left(\frac{\partial\boldsymbol{u}}{\partial t} + \boldsymbol{u}\cdot\boldsymbol{\nabla}\boldsymbol{u}\right) + \boldsymbol{\nabla}p - \boldsymbol{\nabla}\cdot\boldsymbol{\tau}\right]dQ \\
&+ \int_Q \boldsymbol{C} : \left[\frac{\partial\boldsymbol{S}}{\partial t} + \boldsymbol{u}\cdot\boldsymbol{\nabla}\boldsymbol{S} - \boldsymbol{F}(\boldsymbol{S}) - \boldsymbol{G}(\boldsymbol{S})\right]dQ + \int_\Omega \boldsymbol{C}^+ : \left(\boldsymbol{S}^+ - \boldsymbol{S}^-\right)d\Omega \\
&+ \sum_{e=1}^{n_{el}}\int_{Q^e}\tau_{\mathrm{CONS}}\left[\frac{\partial\boldsymbol{C}}{\partial t} + \boldsymbol{u}\cdot\boldsymbol{\nabla}\boldsymbol{C}\right] : \left[\frac{\partial\boldsymbol{S}}{\partial t} + \boldsymbol{u}\cdot\boldsymbol{\nabla}\boldsymbol{S} - \boldsymbol{F}(\boldsymbol{S}) - \boldsymbol{G}(\boldsymbol{S})\right]dQ = 0,
\end{aligned} \tag{15}$$

where $\boldsymbol{C}$, $\boldsymbol{w}$, and q are the weighting functions for the constitutive, momentum, and continuity equations. The space-time slab Q and its boundary P support the basis functions that are continuous in space and discontinuous in time. The 6th and 9th terms in Eq. (15) are the jump terms that weakly impose the continuity of the variables in time. In Eq. (15), we use the following conventions for the space-time elements:

$$\int_Q \cdots dQ = \int_t\int_{\Omega_t} \cdots d\Omega dt, \tag{16}$$

$$\int_P \cdots dP = \int_t\int_{\Gamma_t} \cdots d\Gamma dt. \tag{17}$$

The higher-order derivatives (up to 3rd order) make it cumbersome to solve the Eq. (15). We used two main approaches to handle this issue; 1) integration by parts, and 2) recovery of the terms. Using the integration by parts approach, the higher-order derivatives on the shape (basis) functions can be shifted to the weighting functions. The only consideration with this approach is the additional integrals when the Neumann-type boundary condition is needed. The second approach is to recover the higher-order derivatives by the polynomial field fitting. The fitting algorithm affects the accuracy of the fitted field. The boundary nodes need special treatment for accurate projection. Additionally, the convergence is degraded as a result of the missing Jacobian matrix of the NR iterative scheme.

The sheer amount of terms with higher-order derivatives and nonlinearities necessitate the development of software tools that generate the analytic Jacobian matrices for the NR scheme.

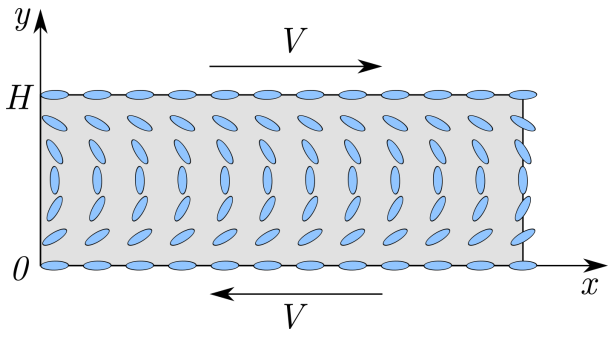

Figure 1. The shear flow schematic; the walls are located at $y = 0, H$.

3 Numerical example

The shear flow problem is defined in Fig. 1 following [11]. We use this test case to validate our stabilized FEM implementation of the microstructured liquid model. The shear flow is assumed between two parallel plates that move in opposite direction by speed V and separated by a gap H. The flow is periodic in the x-direction. The test case is separated into three subsets; homogenous model, decoupled model, and fully-coupled model. For all results that we report here, we assume that the dimensionless viscosity parameter is zero, $\nu_s = 0$. The initial value of the order parameter is assumed to be the equilibrium value of the homogenous case, S_{eq}. On the wall boundaries, the $\boldsymbol{S}$ tensor is aligned with the x-axis (anchored) as,

$$\boldsymbol{S} = S_{eq} \begin{bmatrix} 1 & 0 \\ 0 & -1 \end{bmatrix}, \tag{18}$$

where, $S_{eq} = \frac{1}{2}\sqrt{1 - \frac{4}{3U}}$.

3.1 Homogenous (point) model

In the homogenous case, the 2^{nd} order derivatives (non-homogenous part $\boldsymbol{F}^{\mathrm{nh}}$) are dropped from the constitutive equation (5). The homogenous model simplifies to,

$$\frac{\partial \boldsymbol{S}}{\partial t} = \boldsymbol{F}^{\mathrm{h}}(\boldsymbol{S}) + \boldsymbol{G}(\boldsymbol{S}). \tag{19}$$

The system is decoupled from the momentum equation (1), meaning that the velocity field $\boldsymbol{u}$ is not influenced by the order parameter tensor $\boldsymbol{S}$ or vice versa. The assumptions are: $\frac{\partial}{\partial x} = 0$, $\frac{\partial v}{\partial y} = 0$, and $\frac{\partial u}{\partial y} = 2$. The initial conditions are: $S_{xx} = S_{xy} = 0$. The results are shown in Fig. 2.

3.2 Decoupled model

Here, we solve the full model; the non-homogenous terms (the 2nd order derivatives) are included in the constitutive equation (5). These terms add the long-range elasticity to the model, which is controlled by the Ericksen number Er. This property enables the wall anchoring of $\boldsymbol{S}$. In the decoupled case, the velocity field $\boldsymbol{u}$ is not influenced by the order parameter tensor $\boldsymbol{S}$, and vice versa. The extra-stress equation (13) is dropped from the momentum equation (1).
The gap is $H = 1$. The boundary conditions are; the parallel plates move at speeds $V = \pm 1$, and the order parameter tensor $\boldsymbol{S}$ is aligned with the plates (anchored to the walls). Initially, the flow is fully developed with a constant shear rate of $\frac{\partial u}{\partial y} = 2$, and the $\boldsymbol{S}$ is aligned with the x-axis. The dimensionless parameters are chosen as: $U = 10$, $De = 1$, and $Er = 100$. The time evolution of the order parameter tensor $\boldsymbol{S}$ are shown in Fig. 3.

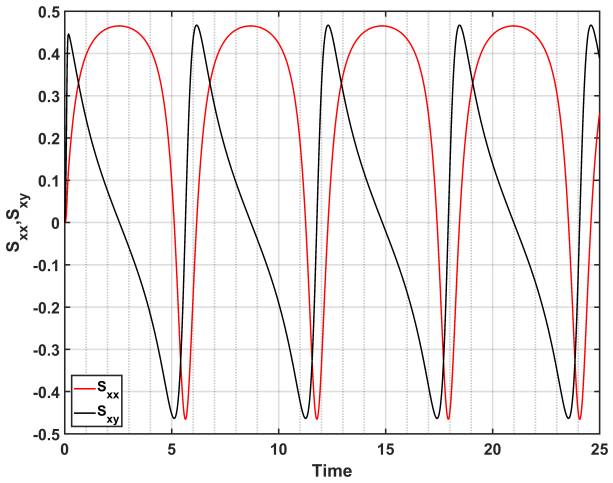

Figure 2. Evolution of the order parameter tensor components for U = 10 and De = 1. These results match those in [11].

3.3 Fully-coupled model

In the fully-coupled model, the extra-stress tensor $\boldsymbol{\tau}$ couples the momentum equation (1) and the constitutive equation (5). We apply the same initial and boundary conditions as in Section 3.2. The dimensionless parameters are chosen as; $U = 10$, $De = 0.1$, and $Er = 100$. The stabilized FEM results are given in Fig. 4.

Conclusions

The GLS3 formulation for the microstructured liquid model was derived in the context of stabilized finite element methods for equal order space-time elements. The higher-order derivatives were handled by the integration by parts and recovery approaches. The analytic Jacobian matrices of the NR scheme were generated by in-house tools. The implementation was validated for various literature data.

Acknowledgements

The authors gratefully acknowledge the computing time granted by the JARA-HPC Vergabegremium on the supercomputer JURECA [10] at Forschungszentrum Jülich.

References

[1] R. H. Baughman. Putting a New Spin on Carbon Nanotubes. *Science*, 290(5495):1310–1311, Nov. 2000.

[2] N. Behabtu, M. J. Green, and M. Pasquali. Carbon nanotube-based neat fibers. *Nano Today*, 3(5):24–34, 2008.

[3] N. Behabtu, C. C. Young, D. E. Tsentalovich, O. Kleinerman, X. Wang, A. W. Ma, E. A. Bengio, R. F. ter Waarbeek, J. J. de Jong, R. E. Hoogerwerf, and others. Strong, light, multifunctional fibers of carbon nanotubes with ultrahigh conductivity. *Science*, 339(6116):182–186, 2013.

[4] M. A. Behr, L. P. Franca, and T. E. Tezduyar. Stabilized finite element methods for the velocity-pressure-stress formulation of incompressible flows. *Computer Methods in Applied Mechanics and Engineering*, 104(1):31–48, 1993.

[5] A. N. Beris and B. J. Edwards. *Thermodynamics of Flowing Systems : With Internal Microstructure*. Oxford University Press, USA, May 1994.

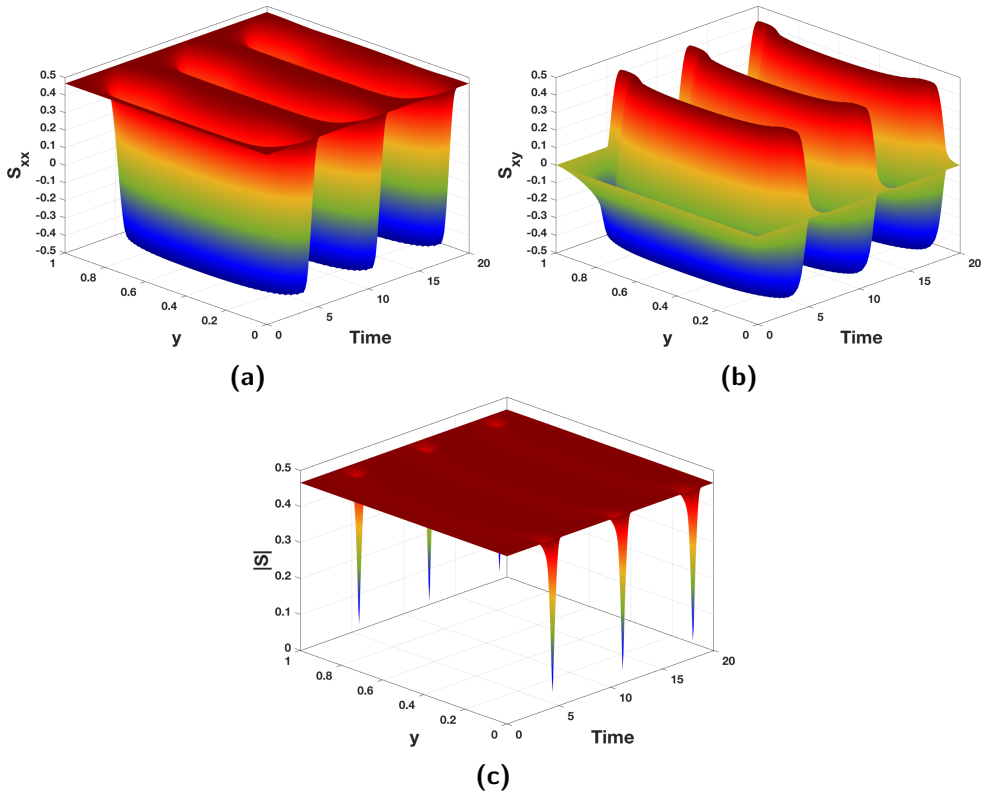

Figure 3. The evolution of (a) S_{xx}, (b) S_{xy}, and (c) $|S|$ for the decoupled model. These results match those in [11].

[6] V. A. Davis, A. N. G. Parra-Vasquez, M. J. Green, P. K. Rai, N. Behabtu, V. Prieto, R. D. Booker, J. Schmidt, E. Kesselman, W. Zhou, H. Fan, W. W. Adams, R. H. Hauge, J. E. Fischer, Y. Cohen, Y. Talmon, R. E. Smalley, and M. Pasquali. True solutions of single-walled carbon nanotubes for assembly into macroscopic materials. *Nature Nanotechnology*, 4(12):830–834, Dec. 2009.

[7] M. Doi and S. F. Edwards. *The Theory of Polymer Dynamics*. Clarendon Press, 1988.

[8] M. J. Green, N. Behabtu, M. Pasquali, and W. W. Adams. Nanotubes as polymers. *Polymer*, 50(21):4979–4997, Oct. 2009.

[9] J. Hone, M. C. Llaguno, N. M. Nemes, A. T. Johnson, J. E. Fischer, D. A. Walters, M. J. Casavant, J. Schmidt, and R. E. Smalley. Electrical and thermal transport properties of magnetically aligned single wall carbon nanotube films. *Applied Physics Letters*, 77(5):666–668, July 2000.

[10] Jülich Supercomputing Centre. JURECA: General-purpose supercomputer at Jülich Supercomputing Centre. *Journal of large-scale research facilities JLSRF*, 2(A62), Mar. 2016.

[11] R. Kupferman, M. N. Kawaguchi, and M. M. Denn. Emergence of structure in a model of liquid crystalline polymers with elastic coupling. *Journal of non-newtonian fluid mechanics*, 91(2):255–271, 2000.

[12] G. Marrucci and F. Greco. The Elastic Constants of Maier-Saupe Rodlike Molecule Nematics. *Molecular Crystals and Liquid Crystals*, 206(1):17–30, Sept. 1991.

[13] L. Onsager. The Effects of Shape on the Interaction of Colloidal Particles. *Annals of the New York Academy of Sciences*, 51(4):627–659, May 1949.

[14] T. E. Tezduyar, S. K. Aliabadi, M. Behr, and S. Mittal. Massively parallel finite element simulation of compressible and incompressible flows. *Computer Methods in Applied Mechanics and Engineering*, 119(1-2):157–177, 1994.

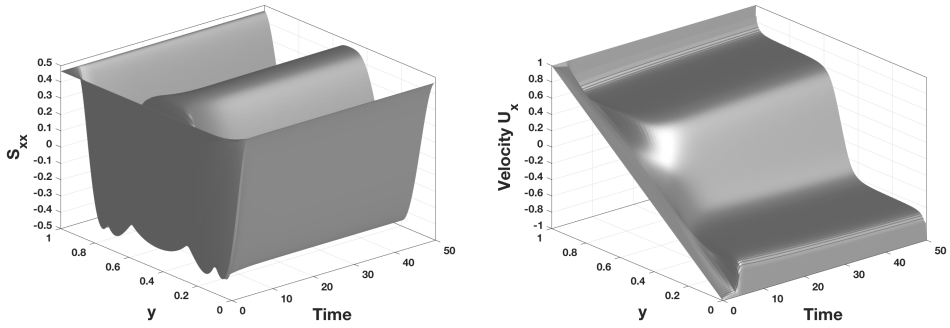

(a) **(b)**

Figure 4. The FEM results of the fully-coupled model for (a) S_{xx}, and (b) V_x. These results are nearly identical to those in [11].